

# Remote Switching of Elastic Movement of Decorated Ligand Nanostructures Controls the Adhesion-Regulated Polarization of Host Macrophages

Ramar Thangam, Myeong Soo Kim, Gunhyu Bae, Yuri Kim, Nayeon Kang, Sungkyu Lee, Hee Joon Jung, Jinhyeok Jang, Hyojun Choi, Na Li, Minjin Kim, Sangwoo Park, Seong Yeol Kim, Thomas Myeongseok Koo, Hong En Fu, Yoo Sang Jeon, Andreja Ambriović-Ristov, Jae-Jun Song, Soo Young Kim, Steve Park, Qiang Wei, Changhyun Ko, Ki-Bum Lee, Ramasamy Paulmurugan, Young Keun Kim,\* and Heemin Kang\*

Design of materials with remote switchability of the movement of decorated nanostructures presenting cell-adhesive Arg-Gly-Asp ligand can decipher dynamic cell-material interactions in decorated ligand nanostructures. In this study, the decoration of ligand-bearing gold nanoparticles (ligand-AuNPs) on the magnetic nanoparticle (MNP) with varying ligand-AuNP densities is demonstrated, which are flexibly coupled to substrate in various MNP densities to maintain constant macroscopic ligand density. Magnetic switching of upward (“Upper Mag”) or downward (“Lower Mag”) movement of varying ligand-AuNPs is shown via stretching and compression of the elastic linker, respectively. High ligand-AuNP densities promote macrophage adhesion-regulated M2 polarization that inhibits M1 polarization. Remote switching of downward movement (“Lower Mag”) of ligand-AuNPs facilitates macrophage adhesion-regulated M2 polarization, which is conversely suppressed by their upward movement (“Upper Mag”), both in vitro and in vivo. These findings are consistent with human primary macrophages. These results provide fundamental understanding into designing materials with decorated nanostructures in both high ligand-AuNP density and downward movement of the ligand-AuNPs toward the substrate to stimulate adhesion-regulated M2 polarization of macrophages while suppressing pro-inflammatory M1 polarization, thereby facilitating tissue-healing responses.


## 1. Introduction

The development of materials that enable the movement of decorated ligand-bearing nanostructures can help to decipher dynamic cellular interactions with native extracellular matrix (ECM)<sup>[1]</sup> exhibiting nanoscale structures and movement of ligands.<sup>[2]</sup> It has been shown that ECM proteins (e.g., collagen) containing cell-adhesive Arg-Gly-Asp (RGD) ligand form macroscopic and nanoscale structures.<sup>[3]</sup> Various tissues, such as bone,<sup>[4]</sup> intervertebral discs,<sup>[5]</sup> and tendons,<sup>[6]</sup> display nanostructures of ligands, such as RGD ligand that dynamically regulate the adhesion and fate of various cell types.<sup>[7]</sup> Various tissues including ligand-bearing nanostructures primarily exhibit movement on the macroscopic and nanoscale. For example, skeletal muscle exhibits flexion and extension,<sup>[8]</sup> lung is subjected to expansion and compression during breathing,<sup>[9]</sup> tendon is subjected to tensile strain during

Dr. R. Thangam, G. Bae, Y. Kim, N. Kang, S. Lee, J. Jang, H. Choi, M. Kim, Dr. S. Park, S. Y. Kim, T. M. Koo, H. E. Fu, Prof. S. Y. Kim, Prof. Y. K. Kim, Prof. H. Kang  
Department of Materials Science and Engineering  
Korea University  
Seoul 02841, Republic of Korea  
E-mail: ykim97@korea.ac.kr; heeminkang@korea.ac.kr

Dr. R. Thangam, M. S. Kim, S. Y. Kim, Dr. Y. S. Jeon  
Institute for High Technology Materials and Devices  
Korea University  
Seoul 02841, Republic of Korea

Dr. H. J. Jung  
Department of Materials Science and Engineering  
Northwestern University  
Evanston, IL 60208, USA

 The ORCID identification number(s) for the author(s) of this article can be found under <https://doi.org/10.1002/adfm.202008698>.

DOI: 10.1002/adfm.202008698

Dr. H. J. Jung  
International Institute for Nanotechnology  
Evanston, IL 60208, USA

Dr. H. J. Jung  
NUANCE Center  
Northwestern University  
Evanston, IL 60208, USA

N. Li, Prof. J.-J. Song  
Department of Otorhinolaryngology-Head and Neck Surgery  
Korea University College of Medicine  
Seoul 08308, Republic of Korea

Dr. S. Park  
Institute of Green Manufacturing Technology  
Korea University  
Seoul 02841, Republic of Korea

physiological loading,<sup>[6]</sup> and myocardium exhibits elastic and contractile movement.<sup>[10]</sup> The native ECM exhibiting nanoscale structures and movement of ligands can dynamically regulate the molecular assembly of adhesion structures<sup>[11]</sup> in macrophages that activate their polarization into pro-inflammatory M1 versus pro-healing M2 phenotypes.<sup>[12]</sup> Indeed, the assembly of cytoskeletal actin and adhesion complex, as well as the elongated spreading of macrophages involving ROCK, are known to activate their M2 polarization.<sup>[13]</sup> These previous reports collectively suggest that the design of materials with remote control of the movement of decorated ligand nanostructures can help to maneuver and decipher the dynamic adhesion and polarization of macrophages regulating immune responses<sup>[14]</sup> to implants toward tissue healing processes.<sup>[15]</sup>

The design of biomaterials that are remotely and temporally controllable via various stimuli, such as light, ultrasound, and magnetic fields, at prescribed time points can manipulate and decipher dynamic interplay between biomaterials and host immune cells in vivo.<sup>[16]</sup> Light illumination can temporally activate photochemical reactions in light-responsive ligand-presenting materials to modulate cellular adhesion.<sup>[17]</sup> However, in vivo application of these materials, particularly in deep tissues, has been limited owing to cytotoxicity exerted by strong light absorption of living tissues. Tissue-penetrative ultrasound can

be applied to generate electricity in piezoelectric materials.<sup>[18]</sup> However, this approach is limited to activating electrically excitable cells, such as neurons. An external magnetic field is highly tissue-penetrating and cytocompatible, and can thus be safely applied to patients.<sup>[19]</sup> Our recent studies have revealed that the application of an external magnetic field can readily control the directional alignment,<sup>[20]</sup> macroscopic movement,<sup>[21]</sup> and nanoscale oscillation<sup>[22]</sup> of magnetic ligand-bearing nanomaterials<sup>[23]</sup> to regulate cellular adhesion. These recent studies have elucidated the effect of separate movement of the individual ligand-bearing nanomaterials<sup>[24]</sup> on dynamically regulating cell adhesion. Developing novel materials allowing the movement of ligand-presenting decorated nanostructures can further advance our regulation and understanding of the dynamic and nanoscale interplay between host immune cells and ligand nanostructures.

In this study, we demonstrate the decoration of AuNPs on the magnetic nanoparticle (MNP) by varying the density of decorated ligand-bearing AuNPs and flexibly couple them to a substrate in various MNP densities to maintain constant macroscopic ligand density (**Scheme 1**). We show magnetic switching of upward (“Upper Mag”) or downward (“Lower Mag”) movement of varying ligand-AuNPs via elastic stretching and compression of the elastic linker, respectively, by moving the MNP decorated with ligand-AuNPs toward a magnet. The nanoscale arrangement<sup>[25]</sup> of the ligand has been primarily designed on a 2D array to help to understand the regulation of cellular adhesion by arranging RGD ligand-presenting nanoparticles<sup>[26]</sup> with varying interparticle spacing and density either statically<sup>[27]</sup> and dynamically,<sup>[28]</sup> microscale and macroscopic density,<sup>[29]</sup> disordering,<sup>[30]</sup> clustering,<sup>[31]</sup> and micropatterns.<sup>[32]</sup> Our present study exploits the movement of ligand-presenting decorated nanostructures to regulate cell adhesion and is thus distinctly different from these previous approaches as well as recent studies demonstrating the movement of non-decorated ligand-bearing nanoparticles.<sup>[20,21b,22]</sup>

Specifically, we increased ligand-AuNP densities when decorating each MNP but decreased the MNP densities during substrate coupling to keep similar macroscopic ligand density in all groups (**Figure 1a**). We designed the size of the ligand-bearing AuNPs (12.5 nm) to be comparable to that of integrin (10 nm) to facilitate the recruitment of individual integrin molecule to each ligand-bearing AuNPs.<sup>[33]</sup> We coated the AuNPs (not MNP) with a long poly(ethylene glycol) (PEG) linker (5 kDa) during substrate coupling to enhance the flexibility of the movement of the MNP.<sup>[34]</sup> We show that high ligand-AuNP density stimulated the adhesion-aided M2 polarization of macrophages involving myosin II, actin polymerization, and ROCK signaling (**Scheme 1**). Conversely, magnetic switching of the upward in situ movement of the MNP decorated AuNPs via linker stretching inhibited macrophage adhesion that induced M1 polarization. On the other hand, low ligand-AuNP density inhibited macrophage adhesion that facilitated M1 polarization. Conversely, magnetic switching of the downward in situ movement of the MNP decorated with AuNPs via linker compression promoted macrophage adhesion that stimulated M2 polarization. Our results were consistent in both in vitro and in vivo settings and with recent reports showing that RGD ligand statically tethered to a substrate via short and long linkers promoted

---

Dr. A. Ambriović-Ristov  
Laboratory for Cell Biology and Signalling  
Division of Molecular Biology  
Ruđer Bošković Institute  
Zagreb 10000, Croatia

Prof. S. Park  
Department of Materials Science and Engineering  
Korea Advanced Institute of Science and Technology (KAIST)  
Daejeon 34141, Republic of Korea

Prof. Q. Wei  
College of Polymer Science and Engineering  
State Key Laboratory of Polymer Materials and Engineering  
Sichuan University  
Chengdu 610065, China

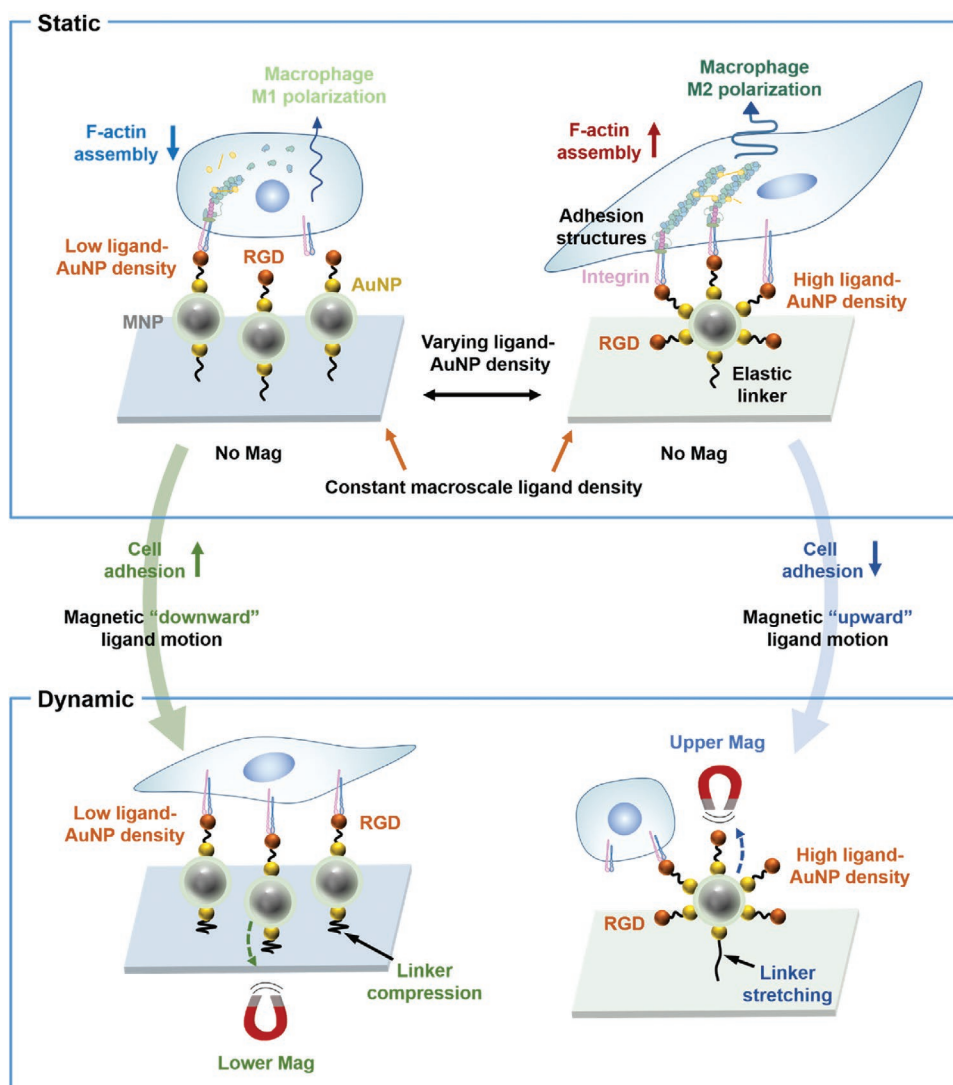
Prof. C. Ko  
Department of Applied Physics  
College of Engineering  
Sookmyung Women's University  
Seoul 04310, Republic of Korea

Prof. K.-B. Lee  
Department of Chemistry and Chemical Biology  
Rutgers University  
Piscataway, NJ 08854, USA

Prof. R. Paulmurugan  
Department of Radiology  
Molecular Imaging Program at Stanford  
Stanford University School of Medicine  
Stanford University  
Palo Alto, CA 94304, USA

Prof. R. Paulmurugan  
Department of Radiology  
Canary Center at Stanford for Cancer Early Detection  
Stanford University School of Medicine  
Stanford University  
Palo Alto, CA 94304, USA

Prof. H. Kang  
Department of Biomicrosystem Technology  
Korea University  
Seoul 02841, Republic of Korea



**Scheme 1.** Schematic summary of experiments in this study. Varying decorated ligand-bearing gold nanoparticles (ligand-AuNPs) on the magnetic nanoparticle (MNP) were flexibly coupled to a substrate without changing macroscopic ligand density. Magnetic switching of the downward (“Lower Mag”) and upward (“Upper Mag”) movement of varying ligand-AuNPs was achieved via compression and stretching of the elastic linker, respectively. High and low ligand-AuNP density under the “No Mag” conditions devoid of the magnet promotes and inhibits the macrophage adhesion-regulated pro-regenerative M2 polarization, respectively, both in vitro and in vivo. Remote downward (“Lower Mag”) and upward (“Upper Mag”) movement of the varying ligand-AuNPs stimulates and suppresses the macrophage adhesion-regulated M2 polarization with the suppression of their M1 polarization, respectively, both in vitro and in vivo.

and inhibited cell adhesion, respectively.<sup>[35]</sup> Furthermore, magnetic switching of the movement of these ligand-presenting decorated nanostructures can effectively regulate the adhesion and resultant polarization of host macrophages to effectively induce pro-healing host responses to implanted biomaterials.

## 2. Results and Discussion

### 2.1. Varying the Decoration of AuNPs on the MNP

To enable magnetic switching of the movement of varying ligand-bearing AuNPs, the MNPs were first synthesized. We prepared the size of the MNP considerably larger than that

of the AuNPs to vary the density of the AuNPs on the surface of the MNP. To allow the decoration of AuNPs, the MNP was amino-functionalized via amino-silica coating. Vibrating sample magnetometry measurement confirmed the reversible magnetic properties of the MNPs with high saturation magnetization ( $M_s$ ) of  $675 \text{ emu g}^{-1}$  (Figure S1, Supporting Information). X-ray diffraction spectra verified the crystalline magnetite phase of the MNPs with the diffraction peaks corresponding to the reference data of crystalline  $\text{Fe}_3\text{O}_4$  phase, such as (220), (311), (400), (422), (511), and (440) planes (Figure S2, Supporting Information). Transmission electron microscopy (TEM) image showed the uniform coating of the amino-silica layer on the MNPs (Figure S3a, Supporting Information). Dynamic light scattering (DLS) analysis confirmed that the diameter of the

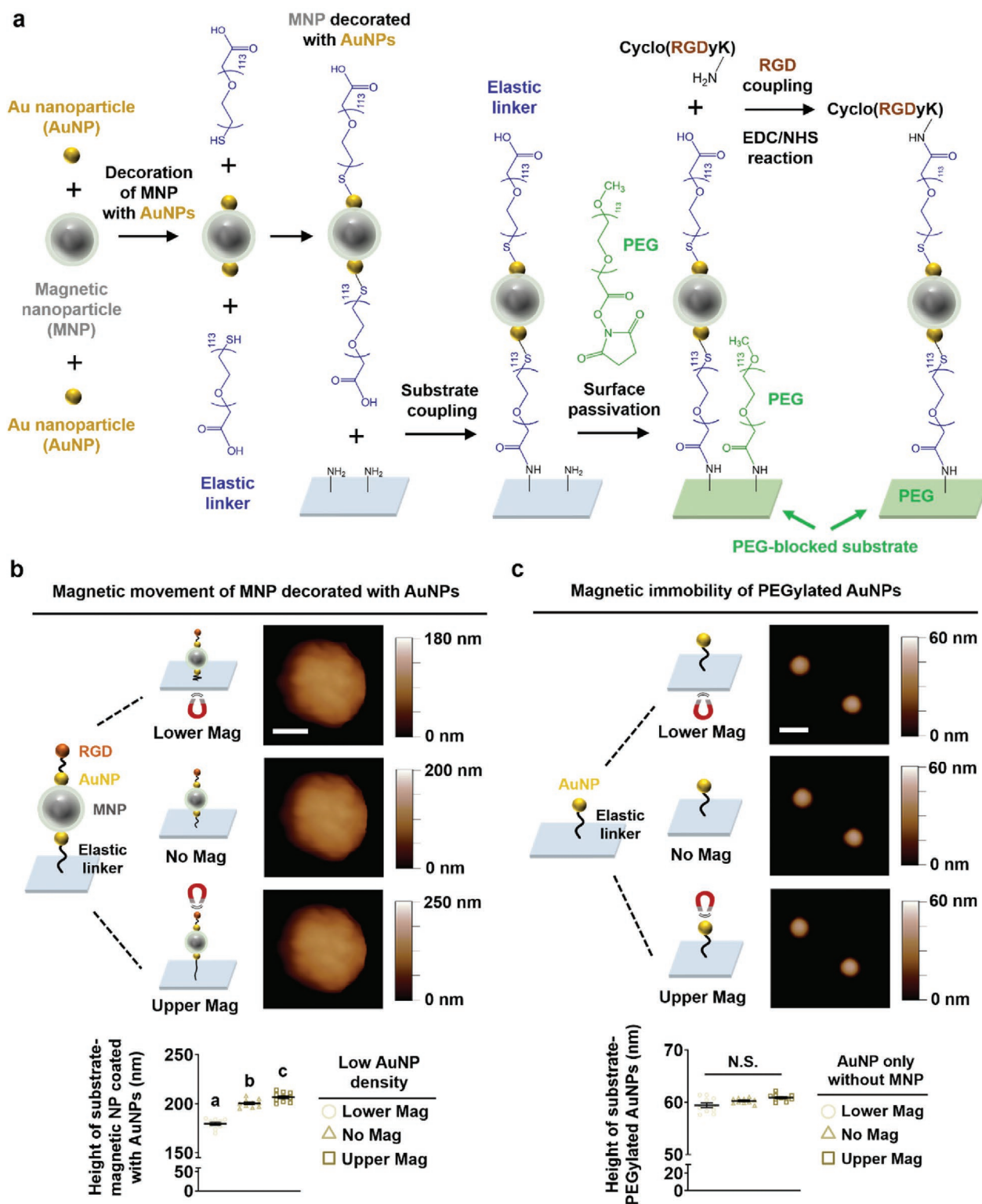


**Figure 1.** Magnetic elastic switching of MNP decorated with AuNPs. a) Schematic illustration of flexible substrate coupling of MNPs decorated with AuNPs to enable in situ magnetic switching of movement (of the ligand-AuNPs). b) Schematic illustration and in situ atomic force microscopy (AFM; scale bar: 100 nm) of magnetically manipulated upward (“Upper Mag”) and downward (“Lower Mag”) movement of the MNP decorated with AuNPs (low AuNP density) through the stretching and compression of the elastic linker, respectively, or in the absence of the magnet (“No Mag”) with corresponding quantification of the height of the MNP decorated with AuNPs. c) AFM images of AuNP alone coupled to a substrate using an elastic linker with corresponding quantification of the height of the AuNP. Data are presented as the mean  $\pm$  standard error ( $n = 10$ ). Statistically significant differences are denoted by different alphabet letters.



MNPs increased from  $179 \pm 13$  to  $210 \pm 19$  nm following coating with the amino-silica layer (Figure S3b, Supporting Information). TEM image and DLS analysis confirmed that AuNPs exhibited a uniform size of  $12.5 \text{ nm} \pm 0.6 \text{ nm}$ , which is substantially smaller than that of the MNP coated with the amino-silica layer (Figure S4a,b, Supporting Information).

The decoration of the AuNPs on the MNP was achieved through the Au-amine reaction and strictly varied by optimizing the reaction concentration of the AuNPs versus the MNP coated with amino-silica to present varying densities of the AuNPs per MNP (Figure 1a). Polyvinylpyrrolidone (PVP) was used to stabilize the decorated AuNPs on the MNP. High-angle annular dark-field scanning transmission electron microscopy (HAADF-STEM) revealed the decorated nanostructures composed of AuNPs (at various densities) uniformly coupled on the surface of the MNP whereas darker and brighter shades indicated MNP and AuNPs, respectively (Figure S5a, Supporting Information). The HAADF-STEM images were used to quantify the surface area and the number of the AuNPs per MNP in the decorated nanostructures. This quantification revealed that the low, moderate, and high AuNP densities (the number of the AuNPs per MNP) were  $39 \pm 6$ ,  $108 \pm 11$ , and  $171 \pm 24$ , respectively (Figure S5b, Supporting Information). The total surface areas of the AuNPs per MNP were  $20\,919 \pm 3064$ ,  $57\,447 \pm 5988$ , and  $90\,789 \pm 12\,530 \text{ nm}^2$ , respectively (Figure S5b, Supporting Information). High-resolution STEM (HR-STEM) verified the atomic arrangement of the crystalline MNP and decorated AuNPs in the nanostructures (Figure S5a, Supporting Information). HR-STEM images verified that the crystalline structures of the MNP and AuNPs were similar to those reported for the crystalline magnetite and gold phase, respectively.

Energy-dispersive X-ray spectroscopy mapping confirmed the uniform distribution of the Au element present in the AuNPs on the surface of the Fe element present in the MNP in the decorated nanostructures (Figure S5a, Supporting Information). UV-Vis absorption spectra also confirmed the decoration of AuNPs on the MNP (Figure S6, Supporting Information). UV-Vis absorption spectra showed the absorption peaks at 520 and 408 nm, corresponding to the AuNPs alone and MNPs alone, respectively. The absorption peaks of the decorated AuNPs on the MNP (at various AuNP densities) overlapped with those of both the AuNPs alone and MNPs alone, which exhibited increasing peak intensities with increasing AuNP densities. DLS analysis revealed that all of the decorated AuNPs on the MNP at various AuNP densities exhibited similar sizes ranging from 207 to 231 nm with no significant differences (Figure S7, Supporting Information).

## 2.2. Flexible Substrate Coupling of Varying Decorated AuNPs without Changing the Macroscopic Ligand Density

Varying decorated AuNPs were coupled to a substrate via serial chemical reactions while keeping the macroscopic ligand density invariant (Figure 1a). An elastic PEG linker (carboxymethyl-PEG-thiol, 5 kDa) was used to coat the surface of the AuNPs on the MNP via Au–S bonds. The PEGylated AuNPs on the surface of the MNPs were coupled to the amine-treated substrate via the EDC/NHS reaction by modulating the reaction time to

display various densities of the MNPs decorated with AuNPs, thereby presenting the constant macroscopic ligand density. To minimize non-RGD ligand-specific macrophage adhesion, the non-MNP-covered area on the amine-treated substrate was passivated with methoxy-PEG-NHS ester. Aminated RGD ligand was then grafted to the PEGylated AuNPs on the surface of the MNP that are coupled on the substrate via the EDC/NHS reaction.

To keep macroscopic ligand density constant, the MNPs decorated with AuNPs at increasing AuNP densities per MNP were coupled to a substrate at decreasing MNP densities by optimizing the reaction time in the substrate coupling. Scanning electron microscopy (SEM) images showed that homogeneous distribution of the PEGylated MNPs decorated with AuNPs at various densities of the MNPs:  $5.2 \pm 0.3$ ,  $2.1 \pm 0.1$ , and  $1.1 \pm 0.1$  particles  $\mu\text{m}^{-2}$  for low, moderate, and high AuNP densities, respectively (Figure S5a, Supporting Information). The total surface areas of the AuNPs per MNP were  $20\,919 \pm 3064$ ,  $57\,447 \pm 5988$ , and  $90\,789 \pm 12\,530 \text{ nm}^2$  (Figure S5b, Supporting Information). Since the AuNPs were coated with RGD ligand, the product of the MNP density and total surface area of the AuNPs per MNP yields macroscopic surface ligand density, which remained similar ( $103\,000$ – $122\,000 \text{ nm}^2 \mu\text{m}^{-2}$ ) without significant differences among the low, moderate, and high AuNP density groups (Figure S5b, Supporting Information). This density of the MNPs decorated with ligand-presenting AuNPs was optimal in the effective regulation of the adhesion and polarization of macrophages by the switching of varying ligand-AuNPs. Fourier transform infrared spectroscopy (FTIR) confirmed serial changes in the chemical bonds after PVP stabilization (C–N bonds at  $1230 \text{ cm}^{-1}$ ) of the MNP decorated with AuNPs, PEGylation (C–O–C bonds at  $1150 \text{ cm}^{-1}$ ), and RGD coupling (amide I and amide II bonds at  $1632 \text{ cm}^{-1}$  and  $1535 \text{ cm}^{-1}$ , respectively) (Figure S8, Supporting Information).

## 2.3. In Situ Magnetic Switching of the Movement of the Ligand-Bearing AuNPs

Next, in situ atomic force microscopy (AFM) imaging was conducted to characterize in situ magnetic switching of the movement of the ligand-bearing AuNPs. By magnetically manipulating the movement of the MNP, upward movement (“Upper Mag”) versus downward movement (“Lower Mag”) of the MNP decorated with ligand-bearing AuNPs were remotely manipulated. We first measured the magnetic field strength as a function of distance from a permanent magnet (270 mT) used in this study (Figure S9, Supporting Information). The AFM imaging was first carried out in the absence of the magnet near the substrate (“No Mag”) (Figure 1b). The permanent magnet was then placed at the upper side of the substrate to induce the upward movement (“Upper Mag”) of the ligand-bearing AuNPs toward the magnet via stretching of the elastic PEG linker. Afterward, the magnet was positioned at the lower side of the substrate to induce the downward movement (“Lower Mag”) of the ligand-bearing AuNPs toward the magnet via compression of the elastic PEG linker.

Utilizing these AFM images, the corresponding changes in the average height and diameter of the MNP decorated

with ligand-bearing AuNPs during their in situ vertical movement were quantified. The heights of the MNP decorated with AuNPs under the “Lower Mag,” “No Mag,” and “Upper Mag” conditions were  $180.0 \pm 2.0$ ,  $195.7 \pm 4.9$ , and  $212.3 \pm 1.5$  nm, and, respectively, thereby confirming that the in situ nanoscale vertical movement of the MNP with AuNPs (Figure 1b). These height differences of 32 nm (between 180 and 212 nm) as a result of using an elastic PEG linker (5 kDa) appeared to be significant to modulate the degree of cells sensing the substrate to markedly alter macrophage adhesion (to be presented in the following text). We also confirmed that the magnet does not induce any changes in the heights of non-magnetically-responsive material (AuNP around 40 nm in diameter that is flexibly or non-flexibly coupled to a substrate) but induces significant changes in the heights of magnetically responsive material (MNP decorated with AuNPs) (Figure 1c, Figures S10 and S11, Supporting Information). In contrast, the diameters of the MNP decorated with AuNPs under the “Lower Mag,” “No Mag,” and “Upper Mag” conditions remained nearly constant, ranging from 243 to 246 nm with no significant differences, thereby confirming no intrinsic changes in the size of the MNP decorated with AuNPs during their in situ movement (Figure S12, Supporting Information). These findings prove that the design of this novel material enabled in situ magnetic switching of the movement of MNP decorated with AuNPs.

#### 2.4. Varying Decorated Ligand-Bearing AuNP Density Alters Macrophage Adhesion

We first evaluated whether varying the ligand-bearing AuNP density (in the “No Mag” condition) can modulate the adhesion of macrophages. We used mouse macrophages (RAW 264.7) to analyze the modulation of their adhesion and polarization. Confocal immunofluorescence images showed that macrophages exhibited more robust adhesion to the substrate with increasing density of the ligand-bearing AuNPs as revealed by pronounced paxillin expression and pervasive F-actin assembly in elongated morphology (Figure 2a). Quantification of the immunofluorescence images further revealed that macrophages adhered to the substrate in higher cell density, spread cell area, cell elongation factor (suggesting elongated spreading of the adherent macrophages), paxillin expression, and F-actin assembly with increasing density of the ligand-AuNPs (Figures S13 and S14, Supporting Information). Our results prove that high ligand-bearing AuNPs density without changing macroscopic RGD ligand density stimulates macrophage adhesion. These results are consistent with a previous finding reporting cell adhesion promoted by nano-clustering of the RGD ligand that resembles high ligand-bearing AuNPs on the MNP.<sup>[31]</sup>

We also performed control experiments without AuNPs or RGD coating on the AuNPs. Confocal immunofluorescence images revealed that macrophages did not readily adhere to the substrate with low adhesion density, low spreading, and round morphology in all groups (no AuNPs or low, moderate, and high AuNP densities without RGD coating) (Figure S15a,b, Supporting Information). We found a similar trend in other control experiments with a coating of non-integrin-specific RGD ligand sequences (scrambled RAD sequences). Macrophages did not

readily adhere to the substrate in all groups (low, moderate, and high AuNP densities with RAD coating) (Figure S16a,b, Supporting Information). These findings indicate the necessity of integrin-specific RGD ligand coated on the AuNPs in the decorated nanostructures to effectively maneuver macrophage adhesion by ligand AuNP density in the decorated nanostructures.

#### 2.5. Magnetic Switching of the Ligand-Bearing AuNPs Regulates Macrophage Adhesion

We next explored whether remote control of in situ switching of varying ligand-AuNPs can maneuver the recruitment of integrin to the decorated ligand nanostructures that regulate adhesion of macrophages. We assessed the adhesion of macrophages under the placement of the magnet at the upper or lower side of the cultures to induce the upward (“Upper Mag”) or downward (“Lower Mag”) in situ movement, respectively, of varying ligand-AuNPs toward the magnet.

We assessed the effect of maneuvering upward or downward movement of the ligand-bearing AuNPs on macrophage adhesion at a low ligand-bearing AuNP density that exhibited a low degree of macrophage adhesion under the “No Mag” condition (Figure S17a,b, Supporting Information). We found that upward movement (“Upper Mag”) of the ligand-bearing AuNPs did not significantly change the degree of macrophage adhesion compared with the “No Mag” condition, which showed a low degree of macrophage adhesion. In stark contrast, downward movement (“Lower Mag”) of ligand-AuNPs significantly promoted macrophage adhesion. Our results are consistent with recent studies showing that RGD ligand statically conjugated to a substrate via a short linker (analogous to our dynamic downward movement of decorated ligand-AuNPs with nano-compressed PEG linker) facilitated cell adhesion.<sup>[35]</sup> On the other hand, we also explored the effect of manipulating the upward or downward movement of the ligand-AuNPs on macrophage adhesion at a high ligand-AuNP density that exhibited a high degree of macrophage adhesion under the “No Mag” condition (Figure S18a,b, Supporting Information). We found that the downward movement of ligand-AuNPs did not significantly change the degree of macrophage adhesion compared with the “No Mag” condition, which exhibited a high degree of macrophage adhesion. In contrast, the upward movement of ligand-bearing AuNPs significantly suppressed macrophage adhesion. Our results are also in good agreement with recent studies showing that RGD ligand grafted to a substrate via a long linker (analogous to our upward movement of decorated ligand-bearing AuNPs with nano-stretched PEG linker) inhibited cell adhesion.<sup>[35]</sup>

We next chose two pairs of groups that exhibited the effective regulation of macrophage adhesion to thoroughly investigate their effect on modulating the adhesion and polarization macrophages both in vitro and in vivo. Specifically, we chose two low ligand-AuNP groups under the “No Mag” and “Lower Mag” conditions and another two high ligand-AuNP groups under the “No Mag” and “Upper Mag” conditions. Confocal immunofluorescence images revealed that the magnetic downward movement of the low ligand-AuNP density group significantly promoted the recruitment of integrin to facilitate macrophage

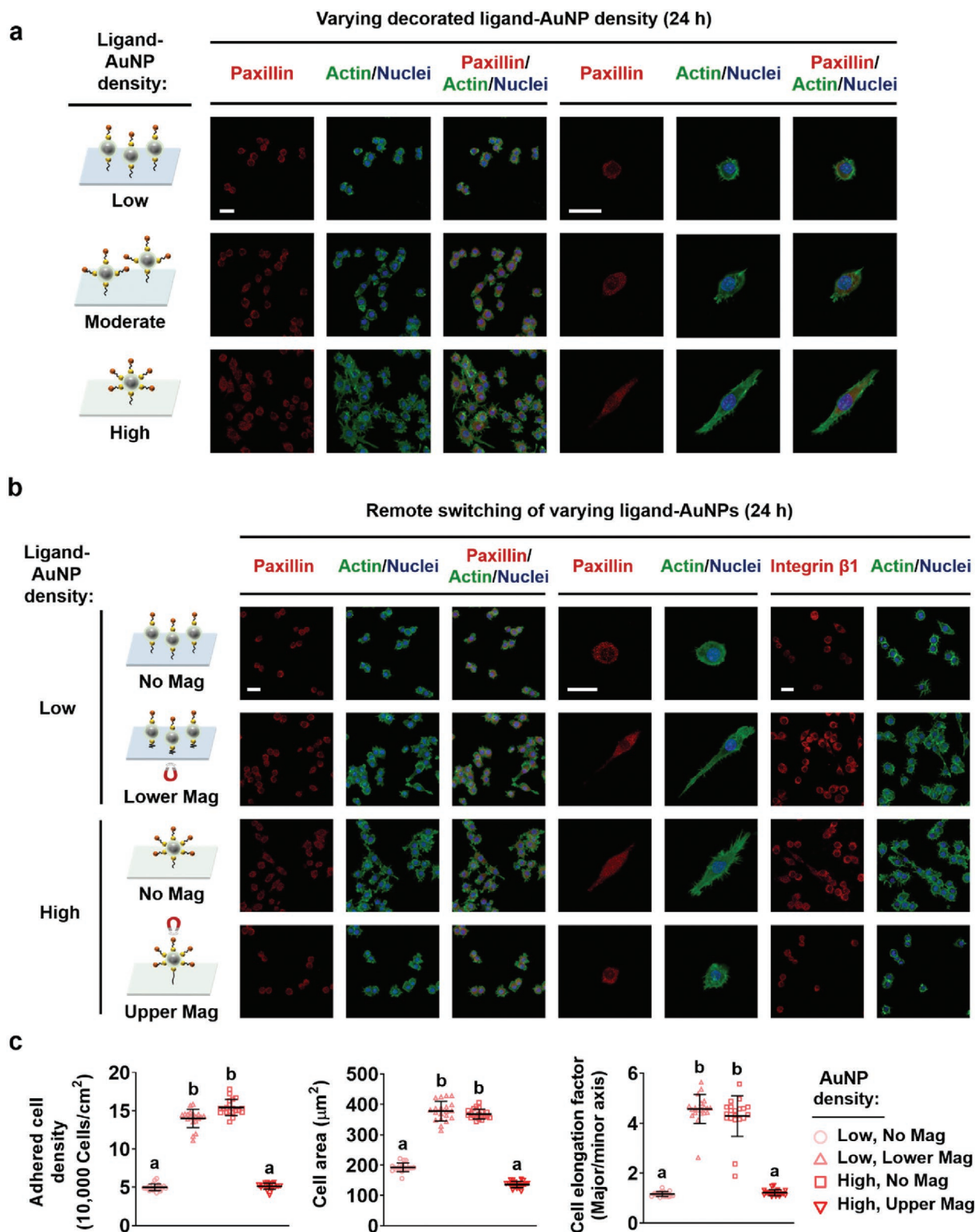


**Figure 2.** High density and downward movement of ligand-bearing AuNPs stimulate macrophage adhesion. Confocal immunofluorescence images of paxillin with F-actin and nuclei in macrophages adhered to the substrate a) under the low, moderate, and high densities of the ligand-AuNPs and b) images of paxillin or integrin  $\beta 1$  with F-actin and nuclei under the switching of varying ligand-AuNPs: low AuNP density (“No Mag” and “Lower Mag”) versus high AuNP density (“No Mag” and “Upper Mag”) with c) corresponding calculations of the adherent macrophage density, spread cell area, and cell elongation factor at 24 h after culture. The scale bar represents 20  $\mu\text{m}$ . Data are presented as the mean  $\pm$  standard error ( $n = 20$ ). Statistically significant differences are indicated by different alphabet letters. All of the experiments reported in (a–c) were repeated twice.

adhesion (Figure 2b,c). On the other hand, confocal immunofluorescence images showed that the magnetic upward movement of the high ligand-AuNP density group significantly inhibited the recruitment of integrin to suppress macrophage adhesion (Figure 2b,c). We also conducted control experiments to explore macrophage adhesion under the switching of varying ligand-AuNPs without RGD ligand or with scrambled RAD sequences. Confocal immunofluorescence images demonstrated that macrophages exhibited low levels of adhesion and a round morphology for the low AuNP density groups (“No Mag” and “Lower Mag”) and high AuNP density groups (“No Mag” and “Upper Mag”) without RGD ligand or with scrambled RAD sequences (Figures S19a,b and S20a,b, Supporting Information). We also confirm that our magnetic switching of varying ligand-bearing AuNPs remains effective when culturing macrophages even after protein coating on the substrate (Figures S21 and S22a,b, Supporting Information).

These findings indicate that integrin-specific RGD ligand coupling on the AuNPs is required to efficiently manipulate the integrin-mediated macrophage adhesion via remote control of in situ switching of varying ligand-AuNPs. Our present study harnessed the movement of ligand-presenting decorated nanostructures to regulate macrophage adhesion, which is distinctly different from other studies that utilized the separate movement of individual ligand-bearing nanoparticles.<sup>[20,21b,22]</sup> Our outcome also provides an insight into the rational design of decorated nanostructured materials in high ligand-AuNP density with their dynamic movement toward the substrate to facilitate macrophage adhesion.

## 2.6. Varying Both the Density and Movement of Ligand-Bearing AuNPs Controls the Adhesion-Regulated Macrophage Polarization

The organization of cytoskeletal actin and integrin-adhesion complex, including paxillin in macrophages resulting in their elongated spreading, has been reported to activate their M2 polarization through ROCK signaling.<sup>[13a-c,e]</sup> These previous reports suggest that the switching of varying ligand-bearing AuNPs can subsequently modulate the adhesion-regulated macrophage polarization. Thus, we next explored such an effect on macrophage polarization in either M1-inducing or M2-inducing medium.

Confocal immunofluorescence images and results from a quantitative gene expression analysis demonstrated that magnetic downward movement (“Lower Mag”) of the ligand-bearing AuNPs at low AuNP density significantly suppressed the expression of iNOS and TNF- $\alpha$  genes as well as TNF- $\alpha$  secretion compared with the “No Mag” condition (Figure 3a and Figure S23, Supporting Information). Furthermore, confocal immunofluorescence images with quantitative gene expression profiles showed that upward movement (“Upper Mag”) of the ligand-bearing AuNPs in high ligand-AuNP density significantly promoted the expression of Arg-1 and Ym1 as well as IL-10 secretion compared with the “No Mag” condition (Figure 3b and Figure S24, Supporting Information). From the control experiments, confocal immunofluorescence images showed that the M2 polarization of macrophages (Arg-1 expression and IL-10 secretion) after culturing in M1-inducing medium and M1 polarization of macrophages (iNOS expression and TNF- $\alpha$  secretion) after culturing in M2-inducing

medium exhibited no significant differences under the switching of varying ligand-AuNPs, thereby suggesting the requirement of appropriate polarization-specific soluble stimuli (Figures S25,S26, Supporting Information). We also found that temporal switching from “No Mag” to “Lower Mag” condition in the low AuNP density group inhibited M1 polarization of macrophages but promoted their M2 polarization (Figures S27a,b and S28a,b, Supporting Information). These findings collectively suggest high density and downward movement of the ligand-AuNPs suppress pro-inflammatory M1 polarization of macrophages but promote their adhesion-dependent pro-healing M2 polarization.

We next deciphered the adhesion-aided M2 polarization of macrophages promoted by high ligand-bearing AuNP density and downward movement of the ligand-bearing AuNPs using specific inhibitors of actin polymerization, myosin II, and ROCK. Our results showed that high density and downward movement of the ligand-AuNPs facilitate ROCK2 expression in macrophages to assemble adhesion structures that stimulate their M2 polarization (Figures S29 and S30, Supporting Information). Our outcome also demonstrated that the inhibition of actin polymerization, myosin II, and ROCK with corresponding inhibitors (cytochalasin D, blebbistatin, and Y27632, respectively) consistently hindered the activation of macrophage adhesion and inhibition of M1 polarization by high ligand-AuNP density and downward movement of the ligand-AuNPs (Figure S31a,b, Supporting Information). Our results further confirmed that the activation of adhesion-regulated M2 polarization in macrophages by high ligand-AuNP density and downward movement of the ligand-AuNPs was consistently hindered by inhibiting actin polymerization, myosin II, and ROCK (Figure S32a,b, Supporting Information). These findings suggest that the molecular machinery of F-actin, myosin II, and ROCK consistently regulates the adhesion and M1 versus M2 polarization under the switching of varying ligand-bearing AuNPs.

## 2.7. Magnetic Switching-Regulated Polarization of Human Macrophages

Next, we used human primary cells via flow cytometry through antibody-based magnetic separation of CD14+ monocytes from CD45+ human peripheral blood mononuclear cells (Figure 4a,b). We further differentiated these CD14+ monocytes into macrophages in the growth media containing granulocyte macrophage-colony stimulating factor and characterized macrophages using specific fluorescent probe-labelled antibodies via flow cytometry (Figure S33a,b, Supporting Information). We found that the “Lower Mag” condition significantly inhibits M1 polarization markers and promotes M2 polarization markers compared to the “No Mag” condition via qRT-PCR-based mRNA expression profiling of human macrophages, similar to our previous findings using mouse macrophages (Figure 4c).

## 2.8. In Vivo Switching of Ligand-Bearing AuNPs Regulates the Adhesion and Polarization of Macrophages

The regulation of macrophage adhesion and pro-healing/anti-inflammatory M2 polarization has been reported to mediate



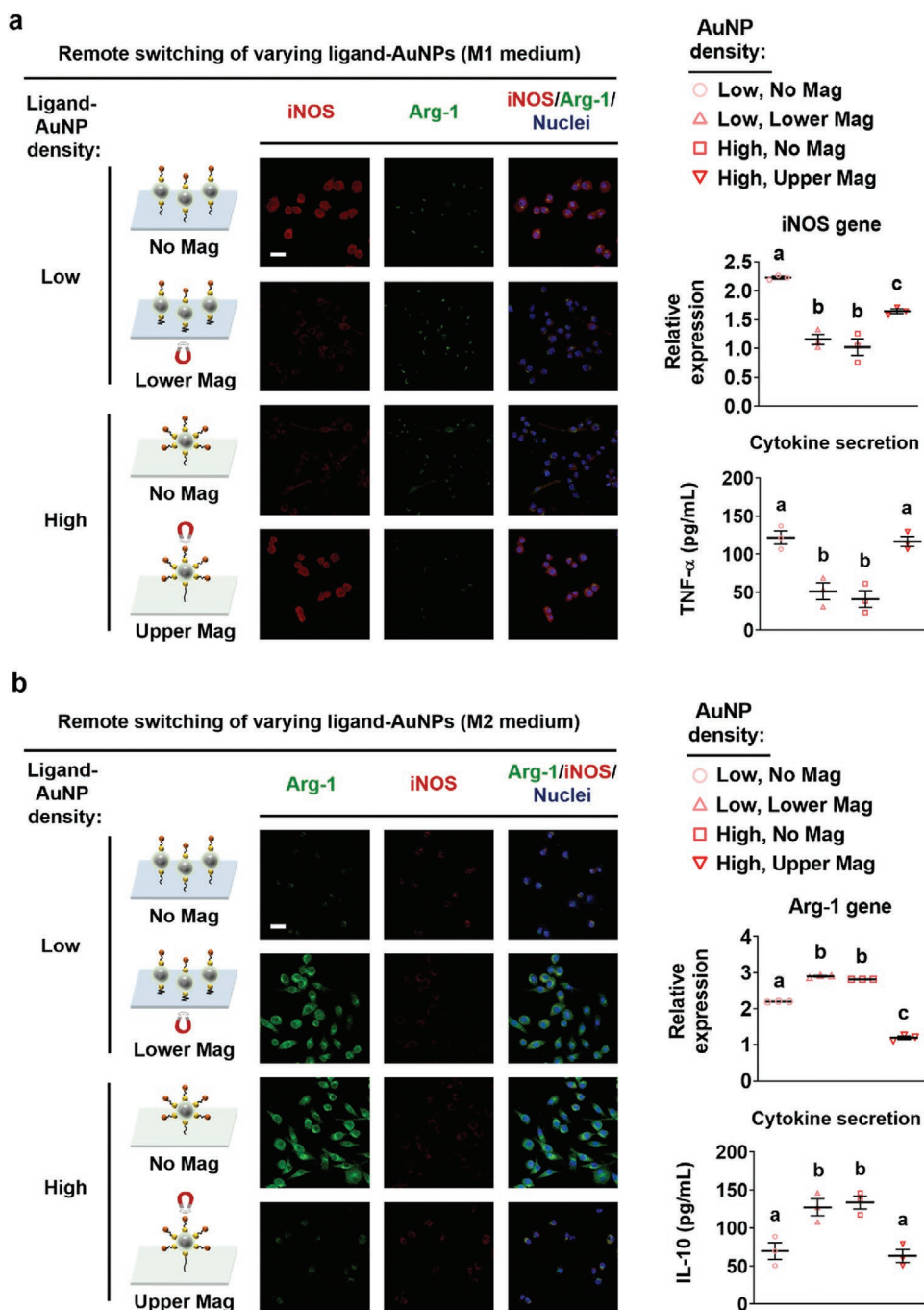


**Figure 3.** High density and downward movement of ligand-bearing AuNPs inhibit M1 polarization of macrophages but facilitate their M2 polarization. a) Confocal immunofluorescence images of iNOS and Arg-1 with nuclei as well as quantitative expression of M1-specific iNOS gene and TNF- $\alpha$  secretion at 36 h after culture in M1-inducing medium or b) confocal immunofluorescence images of Arg-1 and iNOS with nuclei as well as quantitative expression of M2-specific Arg-1 gene and IL-10 secretion at 36 h after culture in M2-inducing medium in macrophages adhered to the substrate under the switching of varying ligand-AuNPs: low AuNP density (“No Mag” and “Lower Mag”) versus high AuNP density (“No Mag” and “Upper Mag”). The scale bar represents 20  $\mu$ m. Data are presented as the mean  $\pm$  standard error ( $n = 3$ ). Statistically significant differences are signified by different alphabet letters. All of the experiments reported in (a,b) were repeated twice.

tissue healing while suppressing inflammation.<sup>[14c,15b,36]</sup> Therefore, to explore in vivo translational effect of ligand-AuNP density and remote switching on the adhesion and polarization of host macrophages, we implanted the substrate presenting MNPs decorated with ligand-bearing AuNPs into

the subcutaneous pockets of mice (Figure 5a). M2-polarizing stimulators [interleukin (IL)-4 and IL-13] were also injected onto the implanted substrate. The permanent magnet was attached to the skin on the backs of the mice (i.e., at the upper side of the substrate) to induce the upward movement (“Upper Mag”)

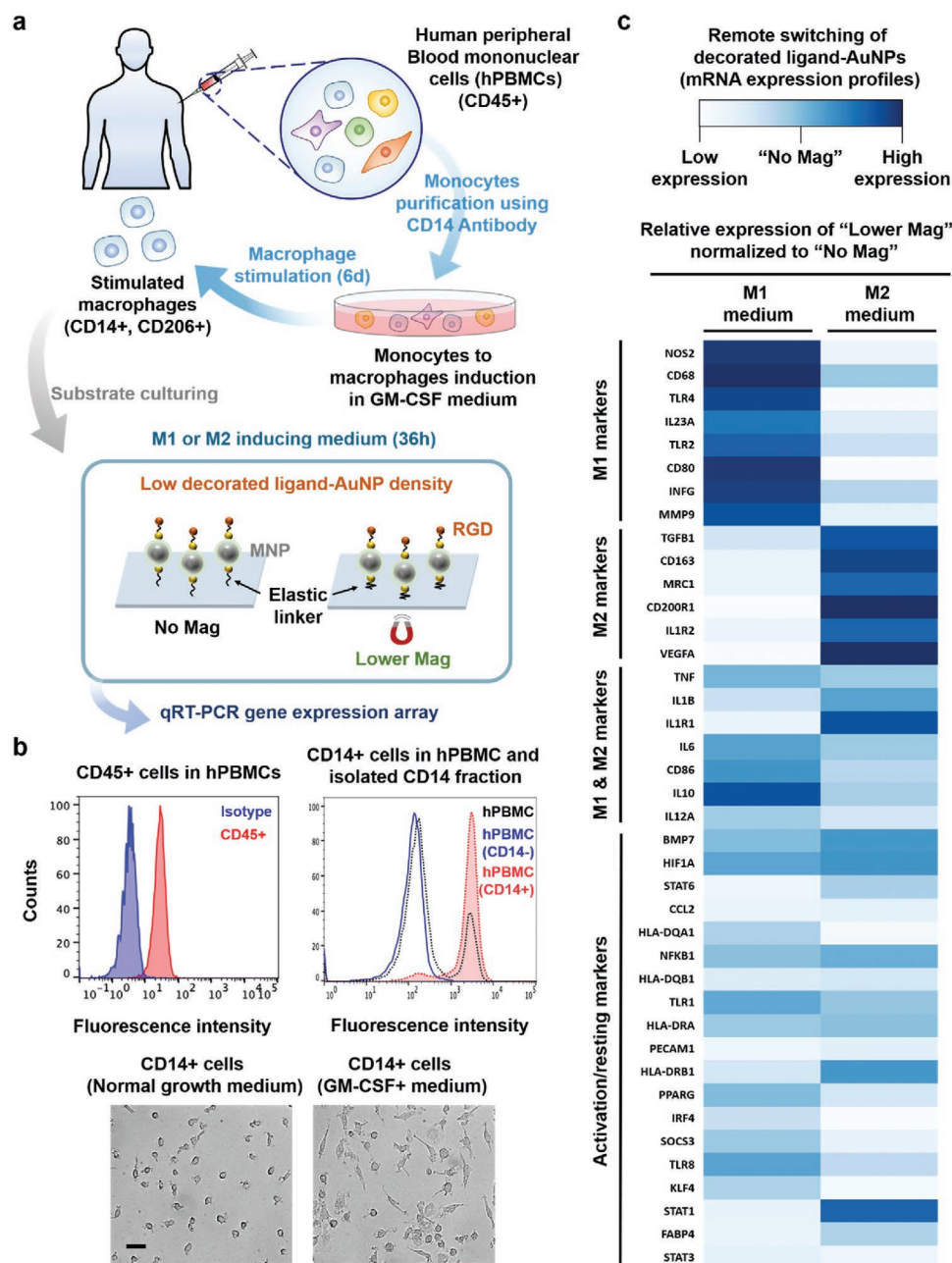


**Figure 4.** Magnetic switching of ligand-bearing AuNPs regulates the polarization of human macrophages. a) Schematic illustration showing the isolation, culturing, and differentiation of monocytes isolated from human primary peripheral blood mononuclear cells (hPBMCs) and associated analysis via flow cytometry and gene expression array. b) Flow cytometry analysis of human peripheral blood mononuclear cells (hPBMCs) and the purified CD14<sup>+</sup> monocytes using specific antibodies (CD45 and CD14) and the microscopic images of CD14<sup>+</sup> monocyte-like macrophages cultured in growth media without and with granulocyte macrophage colony stimulating factor (GM-CSF) for 6 d. Scale bar represents 20  $\mu$ m. c) mRNA expression profiles of human macrophage polarization-related markers from the substrate presenting MNPs decorated with ligand-bearing AuNPs at low AuNP density under magnetic switching ("No Mag" and "Lower Mag") of ligand-AuNPs in both GM-CSF-containing M1- or M2-inducing medium. Relative expression of the "Lower Mag" condition in the heat-map scale is assigned to light blue (low expression) to dark blue colors (high expression) after normalization to "No Mag" condition.

of the MNPs decorated with ligand-AuNPs or to the skin on the abdomens of the mice (i.e., at the lower side of the substrate) to induce their downward movement ("Lower Mag").

Confocal immunofluorescence images with the results of gene expression analysis revealed that magnetic downward

movement ("Lower Mag") of the ligand-bearing AuNPs at low AuNP density substantially promoted the adhesion of host macrophages (in terms of higher cell density and spread cell area) that suppresses M1 polarization (lower TNF- $\alpha$  and iNOS expression) but promotes M2 polarization

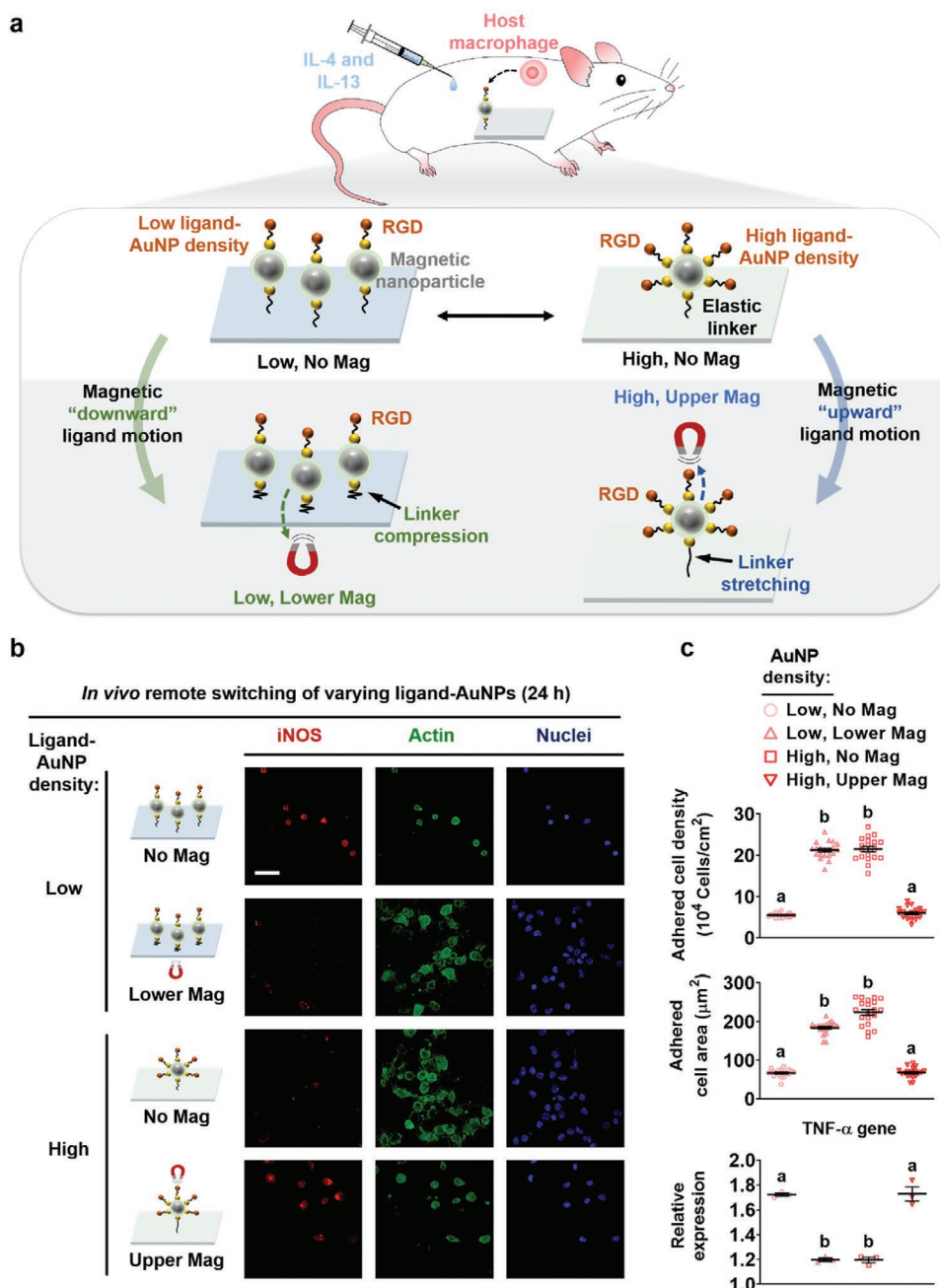
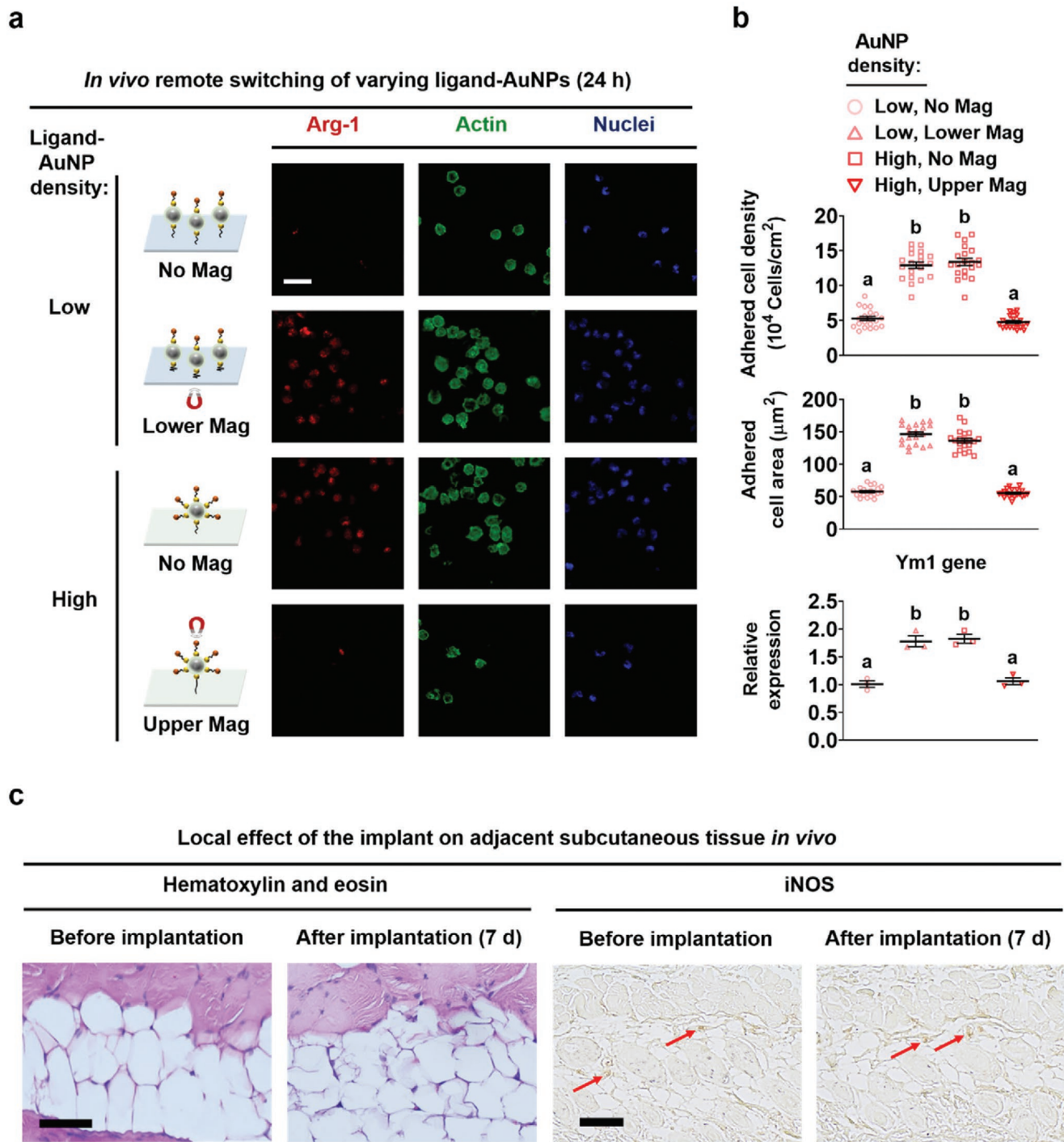


**Figure 5.** High density and downward movement of ligand-bearing AuNPs inhibit the M1 polarization of recruited macrophages in vivo. a) Schematic presentation of switching of varying ligand-AuNPs on the subcutaneously implanted substrate followed by an injection of M2-inducing stimulators. b) Confocal immunofluorescence images of iNOS with F-actin and nuclei in the recruited cells on the implant. c) Corresponding calculations of the adherent macrophage density and spread cell area as well as the quantitative expression of M1-specific gene (TNF- $\alpha$ ) after 24 h under the switching of varying ligand-AuNPs: low AuNP density ("No Mag" and "Lower Mag") versus high AuNP density ("No Mag" and "Upper Mag"). The scale bar represents 20  $\mu\text{m}$ . Data are shown as the mean  $\pm$  standard error ( $n = 10$  for cell density and area quantifications,  $n = 3$  for gene expression quantification). Statistically significant differences are indicated by different alphabet letters. All of the experiments reported in (b,c) were repeated twice.

(higher Ym-1 and Arg-1 expression) compared with the "No Mag" conditions (Figures 5b,c and 6a-b; Figures S34 and S35, Supporting Information). In addition, confocal immunofluorescence images with gene expression profiles demonstrated that upward movement ("Upper Mag") of the ligand-AuNPs at high AuNP density considerably inhibited the adhesion of macrophages (in terms of lower cell density

and spread cell area) that facilitates M1 polarization (higher TNF- $\alpha$  and iNOS expression) but inhibits M2 polarization (higher Ym-1 and Arg-1 expression) compared with the "No Mag" conditions (Figures 5b,c and 6a,b; Figures S34 and S35, Supporting Information). Furthermore, NIMP-R14-positive host neutrophils were found to be recruited on the substrate, which govern the early host response along





**c**

Local effect of the implant on adjacent subcutaneous tissue *in vivo*

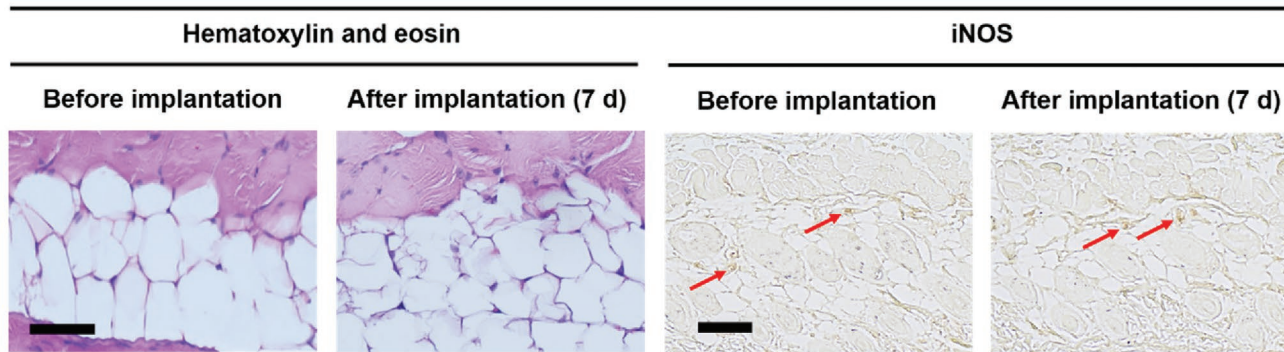


**Figure 6.** High density and downward movement of ligand-bearing AuNPs facilitate macrophage M2 polarization and biocompatible. a) Confocal immunofluorescence images of Arg-1 with F-actin and nuclei in the recruited cells to the subcutaneously implanted substrate followed by injection of M2-inducing stimulators. b) Corresponding quantifications of the adherent macrophage density and spread cell area as well as the quantitative expression of M2-specific gene (Ym1) after 24 h under the switching of varying ligand-AuNPs: low AuNP density (“No Mag” and “Lower Mag”) versus high AuNP density (“No Mag” and “Upper Mag”). The scale bar indicates 20  $\mu\text{m}$ . c) Hematoxylin and eosin staining and immunohistochemical staining for iNOS in the subcutaneous tissue before and after 7 d of subcutaneous implantation of the implant with “No Mag” condition. Arrows indicate iNOS-positive cells. The scale bar represents 200  $\mu\text{m}$ . Data are presented as the mean  $\pm$  standard error ( $n = 10$  for cell density and area quantifications,  $n = 3$  for gene expression quantification). Statistically significant differences are denoted by different alphabet letters. All of the experiments reported in (a–c) were repeated twice.



with macrophages to regulate long-term immune responses (Figure S36, Supporting Information).<sup>[37]</sup>

Our outcome confirms that high density and downward movement of ligand-bearing AuNPs promote the adhesion of the recruited host macrophages that inhibits their M1 polarization. Our results also suggest that high density and downward movement of the ligand AuNPs facilitate the adhesion-regulated pro-healing M2 polarization of the recruited host macrophages. A recent study confirmed that MNPs exert no toxicity to patients.<sup>[38]</sup> H&E staining and immunohistochemical staining for iNOS of surrounding subcutaneous and other tissues confirmed that implants induced minimal toxicity and inflammatory response (Figure 6c and Figure S37, Supporting Information). The implants presenting MNPs decorated with ligand-bearing AuNPs were found to be stable in vivo as evidenced by SEM imaging with no significant degradation or changes in the density of the MNPs decorated with ligand-AuNPs before and after implantation (Figure S37a,b, Supporting Information). Our safe remote switching of the movement of varying ligand-bearing AuNPs to regulate the adhesion and polarization of macrophages requires the examination of anti-inflammatory tissue-healing responses in the long-term period for clinical use.

### 3. Conclusion

We demonstrated the decoration of the AuNPs on the MNP in varying ligand-bearing AuNP densities by varying the reaction concentrations of the AuNPs. We also modulated the reaction time in the flexible substrate coupling of the MNPs decorated with ligand-bearing AuNPs to keep the macroscopic ligand density constant. We demonstrated in situ magnetic switching of the movement of the ligand-bearing AuNPs via the stretching and compression of the elastic linker by in situ magnetic AFM imaging. Our results showed that high density and downward movement of ligand-AuNPs promote the adhesion-regulated M2 polarization of macrophages while inhibiting their M1 polarization involving the molecular switches of myosin II, F-actin, and ROCK. Our results shed fundamental insight that it is beneficial to design decorated nanostructured materials with high ligand density and dynamic movement toward the substrate to elicit tissue healing and inflammation-suppressive responses of implanted materials.

### Supporting Information

Supporting Information is available from the Wiley Online Library or from the author.

### Acknowledgements

R.T. and M.S.K. contributed equally to this work. This work was supported by the National Research Foundation of Korea (NRF) grant funded by the Korea government (Ministry of Science and ICT) (No. 2020R1C1C1011038 and 2019R1A2C3006587). This work was also supported by a Korea University Grant. HAADF-STEM imaging was conducted with the support of the Korea Basic Science Institute. This work made use of the EPIC facility of Northwestern University's

NUANCE Center, which has received support from the Soft and Hybrid Nanotechnology Experimental (SHyNE) Resource (NSF ECCS-1542205), the MRSEC IRG2 program (NSF DMR-1720139) at the Materials Research Center, the International Institute for Nanotechnology (IIN), the Keck Foundation, and the State of Illinois, through the IIN. The surgery was performed after obtaining approval from the Institutional Animal Care and Use Committee at Korea University for "KOREA-2020-0160" under the investigator of Prof. Jae-Jun Song.

### Conflict of Interest

The authors declare no conflict of interest.

### Data Availability Statement

Research data are not shared.

### Keywords

elastic ligand movement, macrophage adhesion, macrophage polarization, magnetic switching, nanoparticle decoration

Received: October 12, 2020

Revised: January 18, 2021

Published online: February 17, 2021

- [1] a) J. Shin, S. Choi, J. H. Kim, J. H. Cho, Y. Jin, S. Kim, S. Min, S. K. Kim, D. Choi, S. W. Cho, *Adv. Funct. Mater.* **2019**, *29*, 1903863; b) J. S. Lee, Y. H. Roh, Y. S. Choi, Y. Jin, E. J. Jeon, K. W. Bong, S. W. Cho, *Adv. Funct. Mater.* **2019**, *29*, 1807803.
- [2] D. C. Kirouac, C. Ito, E. Csaszar, A. Roch, M. Yu, E. A. Sykes, G. D. Bader, P. W. Zandstra, *Mol. Syst. Biol.* **2010**, *6*, 417.
- [3] a) E. Baer, J. J. Cassidy, A. Hiltner, *Pure Appl. Chem.* **1991**, *63*, 961; b) M. J. Dalby, N. Gadegaard, R. O. C. Oreffo, *Nat. Mater.* **2014**, *13*, 558.
- [4] N. Reznikov, R. Shahar, S. Weiner, *Acta Biomater.* **2014**, *10*, 3815.
- [5] J. Cassidy, A. Hiltner, E. Baer, *Connect. Tissue Res.* **1989**, *23*, 75.
- [6] H. R. C. Screen, D. A. Lee, D. L. Bader, J. C. Shelton, *Proc. Inst. Mech. Eng., Part H* **2004**, *218*, 109.
- [7] I. Samarzija, A. Dekanic, J. D. Humphries, M. Paradzik, N. Stojanovic, M. J. Humphries, A. Ambriovic-Ristov, *Cancers* **2020**, *12*, 1910.
- [8] J. E. Drace, N. J. Pelc, *J. Magn. Reson. Imaging* **1994**, *4*, 773.
- [9] G. E. Christensen, J. H. Song, W. Lu, I. El Naqa, D. A. Low, *Med. Phys.* **2007**, *34*, 2155.
- [10] M. J. Ledesma-Carbayo, P. Mahia-Casado, A. Santos, E. Perez-David, M. A. Garcia-Fernandez, M. Desco, *Ultrasound Med. Biol.* **2006**, *32*, 483.
- [11] M. D. Cabezas, B. Meckes, C. A. Mirkin, M. Mrksich, *ACS Nano* **2019**, *13*, 11144.
- [12] a) J. Kim, H. Y. Kim, S. Y. Song, S. H. Go, H. S. Sohn, S. Baik, M. Soh, K. Kim, D. Kim, H. C. Kim, N. Lee, B. S. Kim, T. Hyeon, *ACS Nano* **2019**, *13*, 3206; b) Y. W. Choo, M. Kang, H. Y. Kim, J. Han, S. Kang, J. R. Lee, G. J. Jeong, S. P. Kwon, S. Y. Song, S. Go, M. Jung, J. Hong, B. S. Kim, *ACS Nano* **2018**, *12*, 8977.
- [13] a) F. Y. McWhorter, C. T. Davis, W. F. Liu, *Cell. Mol. Life Sci.* **2015**, *72*, 1303; b) F. Y. McWhorter, T. T. Wang, P. Nguyen, T. Chung, W. F. Liu, *Proc. Natl. Acad. Sci. USA* **2013**, *110*, 17253; c) S. Zandi, S. Nakao, K. H. Chun, P. Fiorina, D. W. Sun, R. Arita, M. Zhao, E. Kim, O. Schueller, S. Campbell, M. Taher, M. I. Melhorn, A. Schering, F. Gatti, S. Tezza, F. Xie, A. Vergani, S. Yoshida, K. Ishikawa,

- M. Yamaguchi, F. Sasaki, R. Schmidt-Ullrich, Y. Hata, H. Enaida, M. Yuzawa, T. Yokomizo, Y. B. Kim, P. Sweetnam, T. Ishibashi, A. Hafezi-Moghadam, *Cell Rep.* **2015**, *10*, 1173; d) V. Ballotta, A. Driessen-Mol, C. V. C. Bouten, F. P. T. Baaijens, *Biomaterials* **2014**, *35*, 4919; e) T. D. Zaveri, J. S. Lewis, N. V. Dolgova, M. J. Clare-Salzler, B. G. Keselowsky, *Biomaterials* **2014**, *35*, 3504.
- [14] a) K. S. Kim, J. Y. Lee, J. Han, H. S. Hwang, J. Lee, K. Na, *Adv. Funct. Mater.* **2019**, *29*, 1900773; b) R. J. C. Bose, N. Tharmalingam, F. J. G. Marques, U. K. Sukumar, A. Natarajan, Y. T. Zeng, E. Robinson, A. Bermudez, E. Chang, F. Habte, S. J. Pitteri, J. R. McCarthy, S. S. Gambhir, T. F. Massoud, E. Mylonakis, R. Paulmurugan, *ACS Nano* **2020**, *14*, 5818; c) O. Veiseh, J. C. Doloff, M. L. Ma, A. J. Vegas, H. H. Tam, A. R. Bader, J. Li, E. Langan, J. Wyckoff, W. S. Loo, S. Jhunjhunwala, A. Chiu, S. Siebert, K. Tang, J. Hollister-Lock, S. Aresta-Dasilva, M. Bochenek, J. Mendoza-Elias, Y. Wang, M. Qi, D. M. Lavin, M. Chen, N. Dholakia, R. Thakrar, I. Lacik, G. C. Weir, J. Oberholzer, D. L. Greiner, R. Langer, D. G. Anderson, *Nat. Mater.* **2015**, *14*, 643; d) H. Y. Kim, M. Kang, Y. W. Choo, S. H. Go, S. P. Kwon, S. Y. Song, H. S. Sohn, J. Hong, B. S. Kim, *Nano Lett.* **2019**, *19*, 5185; e) H. T. Ruan, Q. Y. Hu, D. Wen, Q. Chen, G. J. Chen, Y. F. Lu, J. Q. Wang, H. Cheng, W. Y. Lu, Z. Gu, *Adv. Mater.* **2019**, *31*, 1806957; f) H. R. Wang, X. Han, Z. L. Dong, J. Xu, J. Wang, Z. Liu, *Adv. Funct. Mater.* **2019**, *29*, 1902440; g) Y. Chao, Q. Chen, Z. Liu, *Adv. Funct. Mater.* **2020**, *30*, 1902785; h) L. He, T. Nie, X. Xia, T. Liu, Y. Huang, X. Wang, T. Chen, *Adv. Funct. Mater.* **2019**, *29*, 1901240.
- [15] a) J. W. Godwin, A. R. Pinto, N. A. Rosenthal, *Proc. Natl. Acad. Sci. USA* **2013**, *110*, 9415; b) K. Sadtler, A. Singh, M. T. Wolf, X. K. Wang, D. M. Pardoll, J. H. Elisseeff, *Nat. Rev. Mater.* **2016**, *1*, 16040; c) K. Sadtler, K. Estrellas, B. W. Allen, M. T. Wolf, H. N. Fan, A. J. Tam, C. H. Patel, B. S. Lubber, H. Wang, K. R. Wagner, J. D. Powell, F. Housseau, D. M. Pardoll, J. H. Elisseeff, *Science* **2016**, *352*, 366.
- [16] a) Y. Kim, H. Choi, J. E. Shin, G. Bae, R. Thangam, H. Kang, *View* **2020**, *1*, 20200029; b) B. S. Gomes, B. Simoes, P. M. Mendes, *Nat. Rev. Chem.* **2018**, *2*, 0120.
- [17] a) T. T. Lee, J. R. Garcia, J. I. Paez, A. Singh, E. A. Phelps, S. Weis, Z. Shafiq, A. Shekaran, A. del Campo, A. J. Garcia, *Nat. Mater.* **2015**, *14*, 352; b) W. Li, J. S. Wang, J. S. Ren, X. G. Qu, *J. Am. Chem. Soc.* **2014**, *136*, 2248; c) W. Li, Z. W. Chen, L. Zhou, Z. H. Li, J. S. Ren, X. G. Qu, *J. Am. Chem. Soc.* **2015**, *137*, 8199; d) L. F. Kadem, M. Holz, K. G. Suana, Q. Li, C. Lamprecht, R. Herges, C. Selhuber-Unkel, *Adv. Mater.* **2016**, *28*, 1799.
- [18] A. Marino, S. Arai, Y. Y. Hou, E. Sinibaldi, M. Pellegrino, Y. T. Chang, B. Mazzolai, V. Mattoli, M. Suzuki, G. Ciofani, *ACS Nano* **2015**, *9*, 7678.
- [19] a) M. Prothmann, F. von Knobelsdorff-Brenkenhoff, A. Topper, M. A. Dieringer, E. Shahid, A. Graessl, J. Rieger, D. Lysiak, C. Thalhammer, T. Huelnhagen, P. Kellman, T. Niendorf, J. Schulz-Menger, *PLoS One* **2016**, *11*, e0148066; b) T. H. Shin, S. Kang, S. Park, J. S. Choi, P. K. Kim, J. Cheon, *Nat. Protoc.* **2018**, *13*, 2664; c) M. Colombo, S. Carregal-Romero, M. F. Casula, L. Gutierrez, M. P. Morales, I. B. Bohm, J. T. Heverhagen, D. Prospero, W. J. Parak, *Chem. Soc. Rev.* **2012**, *41*, 4306; d) G. T. Yu, L. Rao, H. Wu, L. L. Yang, L. L. Bu, W. W. Deng, L. Wu, X. L. Nan, W. F. Zhang, X. Z. Zhao, W. Liu, Z. J. Sun, *Adv. Funct. Mater.* **2018**, *28*, 1801389.
- [20] S. Min, Y. S. Jeon, H. J. Jung, C. Khatua, N. Li, G. Bae, H. Choi, H. Hong, J. E. Shin, M. J. Ko, H. S. Ko, I. Jun, H. E. Fu, S. H. Kim, R. Thangam, J. J. Song, V. P. Dravid, Y. K. Kim, H. Kang, *Adv. Mater.* **2020**, *30*, 2004300.
- [21] a) H. Choi, G. Bae, C. Khatua, S. Min, H. J. Jung, N. Li, I. Jun, H. W. Liu, Y. Cho, K. H. Na, M. Ko, H. Shin, Y. H. Kim, S. Chung, J. J. Song, V. P. Dravid, H. Kang, *Adv. Funct. Mater.* **2020**, *30*, 2001446; b) C. Khatua, S. Min, H. J. Jung, J. E. Shin, N. Li, I. Jun, H. W. Liu, G. Bae, H. Choi, M. J. Ko, Y. S. Jeon, Y. J. Kim, J. Lee, M. Ko, G. Shim, H. Shin, S. Lee, S. Chung, Y. K. Kim, J. J. Song, V. P. Dravid, H. Kang, *Nano Lett.* **2020**, *20*, 4188.
- [22] H. Kang, D. S. H. Wong, X. H. Yan, H. J. Jung, S. Kim, S. Lin, K. C. Wei, G. Li, V. P. Dravid, L. M. Bian, *ACS Nano* **2017**, *11*, 9636.
- [23] H. Kang, K. Y. Zhang, H. J. Jung, B. G. Yang, X. Y. Chen, Q. Pan, R. Li, X. Y. Xu, G. Li, V. P. Dravid, L. M. Bian, *Adv. Mater.* **2018**, *30*, 1803591.
- [24] J. H. Lee, H. K. Choi, L. Yang, S. T. D. Chueng, J. W. Choi, K. B. Lee, *Adv. Mater.* **2018**, *30*, 1802762.
- [25] S. G. Higgins, M. Becce, A. Belessiotis-Richards, H. Seong, J. E. Sero, M. M. Stevens, *Adv. Mater.* **2020**, *32*, 1903862.
- [26] F. F. Meng, J. P. Wang, Q. N. Ping, Y. Yeo, *ACS Nano* **2018**, *12*, 6458.
- [27] a) X. Wang, S. Y. Li, C. Yan, P. Liu, J. D. Ding, *Nano Lett.* **2015**, *15*, 1457; b) K. Ye, X. Wang, L. P. Cao, S. Y. Li, Z. H. Li, L. Yu, J. D. Ding, *Nano Lett.* **2015**, *15*, 4720.
- [28] J. Deng, C. S. Zhao, J. P. Spatz, Q. Wei, *ACS Nano* **2017**, *11*, 8282.
- [29] J. A. Deeg, I. Louban, D. Aydin, C. Selhuber-Unkel, H. Kessler, J. P. Spatz, *Nano Lett.* **2011**, *11*, 1469.
- [30] J. H. Huang, S. V. Grater, F. Corbellin, S. Rinck, E. Bock, R. Kemkemer, H. Kessler, J. D. Ding, J. P. Spatz, *Nano Lett.* **2009**, *9*, 1111.
- [31] L. Y. Koo, D. J. Irvine, A. M. Mayes, D. A. Lauffenburger, L. G. Griffith, *J. Cell Sci.* **2002**, *115*, 1423.
- [32] C. S. Chen, M. Mrksich, S. Huang, G. M. Whitesides, D. E. Ingber, *Science* **1997**, *276*, 1425.
- [33] J.-P. Xiong, T. Stehle, R. Zhang, A. Joachimiak, M. Frech, S. L. Goodman, M. A. Arnaout, *Science* **2002**, *296*, 151.
- [34] B. Pelaz, P. del Pino, P. Maffre, R. Hartmann, M. Gallego, S. Rivera-Fernandez, J. M. de la Fuente, G. U. Nienhaus, W. J. Parak, *ACS Nano* **2015**, *9*, 6996.
- [35] a) B. Trappmann, J. E. Gautrot, J. T. Connelly, D. G. T. Strange, Y. Li, M. L. Oyen, M. A. C. Stuart, H. Boehm, B. J. Li, V. Vogel, J. P. Spatz, F. M. Watt, W. T. S. Huck, *Nat. Mater.* **2012**, *11*, 642; b) S. J. Attwood, E. Cortes, A. W. M. Haining, B. Robinson, D. Y. Li, J. Gautrot, A. D. Hernandez, *Sci. Rep.* **2016**, *6*, 34334.
- [36] J. M. Anderson, A. Rodriguez, D. T. Chang, *Semin. Immunol.* **2008**, *20*, 86.
- [37] J. Han, Y. S. Kim, M. Y. Lim, H. Y. Kim, S. Kong, M. Kang, Y. W. Choo, J. H. Jun, S. Ryu, H. Y. Jeong, J. Park, G. J. Jeong, J. C. Lee, G. H. Eom, Y. Ahn, B. S. Kim, *ACS Nano* **2018**, *12*, 1959.
- [38] K. Maier-Hauff, F. Ulrich, D. Nestler, H. Niehoff, P. Wust, B. Thiesen, H. Orawa, V. Budach, A. Jordan, *J. Neuro-Oncol.* **2011**, *103*, 317.